

# Advanced Functional Materials

## Direct Observation of Ferroelectric Domain Walls in LiNbO<sub>3</sub>: Wall-Meanders, Kinks, and Local Electric Charges --Manuscript Draft--

Manuscript Number:	
Full Title:	Direct Observation of Ferroelectric Domain Walls in LiNbO <sub>3</sub> : Wall-Meanders, Kinks, and Local Electric Charges
Article Type:	Full Paper
Section/Category:	
Keywords:	Characterization Tools; Ferroics; Structure-Property Relationships; Patterning.
Corresponding Author:	Dominique Schryvers, Ph.D. University of Antwerp BELGIUM
Additional Information:	
Question	Response
<p>Please submit a plain text version of your cover letter here.</p> <p><b>If you are submitting a revision of your manuscript, please do not overwrite your original cover letter. There is an opportunity for you to provide your responses to the reviewers later; please do not add them here.</b></p>	<p>We believe that future functional device materials will not operate as bulk materials but will be based on nano-structures inside the bulk. The relevant scientific field is 'Domain Boundary Engineering' where twin boundaries, domain glasses, Bloch walls etc. are the actual devices embedded inside some ferroic matrix. This development requires a very good understanding of the geometrical nature of domain boundaries. The main breakthrough was our earlier paper on the polarity of twin boundaries in CaTiO<sub>3</sub> which is highly cited (ADVANCED MATERIALS 24 523 Published: JAN 24 2012). Ferroelectric 180 degree boundaries were largely excluded from such investigations because of two reasons: firstly it was generally assumed that domain walls would be straight and uncharged; secondly, the experimental difficulties to observe such domain boundaries are pretty horrendous so that several previous attempts by other groups failed.</p> <p>In the manuscript we show the first direct observation of 180 degree walls in LiNbO<sub>3</sub> ever. We clearly show that walls are not straight on a local level (but globally pretty straight if a small thickness is considered). Furthermore, we show that the walls are indeed charged. Local excess charges populate the walls simply because the walls meander and each kink contains a charge. This is a major breakthrough which can now be used to construct walls with lots of meanders and hence high carrier densities and hence lead to novel device fabrications.</p> <p>We trust this work will be very relevant to the readers of Advanced Functional Materials.</p>
Corresponding Author Secondary Information:	
Corresponding Author's Institution:	University of Antwerp
Corresponding Author's Secondary Institution:	
First Author:	Julie Gonnissen
First Author Secondary Information:	
Order of Authors:	Julie Gonnissen Dmitry Batuk Guillaume F. Nataf Lewys Jones Artem M. Abakumov Sandra Van Aert

	Dominique Schryvers
	Ekhard K. H. Salje
<b>Order of Authors Secondary Information:</b>	
<b>Abstract:</b>	<p>Direct observations of the ferroelectric domain boundaries in LiNbO<sub>3</sub> are performed using high resolution HAADF-STEM imaging revealing a very narrow width of the domain wall between the 180° domains. The domain walls demonstrate local side-way meandering, which results in inclinations even when the overall wall orientation follows the ferroelectric polarization. These local meanders contain kinks with "head-to-head" and "tail-to-tail" dipolar configurations and are therefore locally charged. The charged meanders are confined to a few cation layers along the polarization direction and are separated by longer stretches of straight domain walls.</p>

DOI: 10.1002/

**Article type: Full paper**

**Direct Observation of Ferroelectric Domain Walls in LiNbO<sub>3</sub>: Wall-Meanders, Kinks, and Local Electric Charges**

*Julie Gonnissen, Dmitry Batuk, Guillaume F. Nataf, Lewys Jones, Artem M. Abakumov, Sandra Van Aert, Dominique Schryvers\*, Ekhard K. H. Salje*

J. Gonnissen, Dr. D. Batuk, Prof. A. M. Abakumov, Prof. S. Van Aert, Prof. D. Schryvers  
Electron Microscopy for Materials Science (EMAT), University of Antwerp,  
Groenenborgerlaan 171, 2020 Antwerp, Belgium.  
E-mail: Nick.Schryvers@uantwerpen.be

Prof. E. K. H. Salje  
Department of Earth Sciences, University of Cambridge,  
Downing Street, Cambridge CB1 3EQ, UK

G. F. Nataf  
Materials Research and Technology Department, Luxembourg Institute of Science  
and Technology, 41 rue du Brill, L-4422 Belvaux, Luxembourg  
SPEC, CEA, CNRS, Université Paris-Saclay,  
CEA Saclay, 91191 Gif-sur-Yvette, France

Dr. L. Jones  
Department of Materials, University of Oxford,  
Parks Road, Oxford OX1 3PH, United Kingdom

Prof. A. M. Abakumov  
Center for Electrochemical Energy Storage, Skolkovo Institute of Science and  
Technology, Nobelya str. 3, 143026 Moscow, Russia

**Keywords :** Characterization Tools, Ferroics, Structure-Property Relationships,  
Patterning

1  
2  
3  
4  
5  
6  
7  
8  
9  
10  
11  
12  
13  
14  
15  
16  
17  
18  
19  
20  
21  
22  
23  
24  
25  
26  
27  
28  
29  
30  
31  
32  
33  
34  
35  
36  
37  
38  
39  
40  
41  
42  
43  
44  
45  
46  
47  
48  
49  
50  
51  
52  
53  
54  
55  
56  
57  
58  
59  
60  
61  
62  
63  
64  
65

# ABSTRACT:

Direct observations of the ferroelectric domain boundaries in  $\text{LiNbO}_3$  are performed using high resolution HAADF-STEM imaging revealing a very narrow width of the domain wall between the  $180^\circ$  domains. The domain walls demonstrate local side-way meandering, which results in inclinations even when the overall wall orientation follows the ferroelectric polarization. These local meanders contain kinks with “head-to-head” and “tail-to-tail” dipolar configurations and are therefore locally charged. The charged meanders are confined to a few cation layers along the polarization direction and are separated by longer stretches of straight domain walls.

## 1. Introduction

Ferroic domain walls can be functional elements of a material while the same functionality does not exist in the bulk.<sup>[1]</sup> Typical examples are conducting domain walls in  $\text{BiFeO}_3$ <sup>[2-4]</sup>,  $\text{Pb}(\text{Zr,Ti})\text{O}_3$ <sup>[5]</sup>, superconducting twin walls in  $\text{WO}_3$ <sup>[6,7]</sup>, polarity and ferroelectricity in ferroelastic domain walls in  $\text{CaTiO}_3$  and  $\text{SrTiO}_3$ <sup>[8-11]</sup>, and segregation of chemical species in domain walls.<sup>[1,12]</sup> Direct structural observations of displacements inside domain walls are rare, however.<sup>[9,13,14]</sup> It is even harder to show fine structures, such as additional symmetry breaking, inside domain walls. The only reported case is the polarity in twin walls in  $\text{CaTiO}_3$  revealed by high resolution transmission electron microscopy observations.<sup>[9]</sup>

Ferroelectric walls in  $\text{LiNbO}_3$  are expected to display transport functionality: the walls are locally electrically charged, while the bulk is known not to contain any electric charges besides those related to point defects. These walls are expected to be electrically conducting when the carrier concentration is sufficiently large.<sup>[15-18]</sup> Ferroelectric walls in  $\text{LiNbO}_3$  separate domains with the polarizations pointing in opposite directions ( $180^\circ$  walls). The geometrical condition for charged walls is that they are inclined with respect to the equilibrium direction along the ferroelectric polarization direction  $[0001]$  (in the hexagonal setting).<sup>[15-17]</sup>

Such inclined and conductive walls have previously been observed in  $\text{Pb}(\text{Zr,Ti})\text{O}_3$  thin films<sup>[19]</sup> and calculations demonstrate that the static conductivity drastically increases at inclined domain walls, even for small inclination angles.<sup>[18]</sup> Electron microscopy has shown that charged domain walls, particularly in the most extreme case of a head-to-head or tail-to-tail configuration, act as barriers for defect movements.<sup>[20-26]</sup> Inclined walls generate local strain in the nearby bulk, while walls in mechanical equilibrium are neither charged nor do they strain the lattice. However,

1 LiNbO<sub>3</sub> with macroscopically non-inclined walls still contains significant defect  
2 structures<sup>[20,27-29]</sup> which decorate the walls.<sup>[30,31]</sup> Nataf et al. argued that even ‘straight’  
3 walls should show local inclinations, they ‘meander’, so that head-to-head and tail-to-  
4 tail dipolar kink configurations occur locally.<sup>[24]</sup> Each such configuration represents  
5 an increase or decrease of carrier concentrations and hence corresponds to a local  
6 charge monopole.  
7

8  
9  
10  
11  
12  
13  
14 LiNbO<sub>3</sub> has a trigonal structure with the  $R\bar{3}c$  space group in the paraelectric  
15 phase. With the onset of ferroelectricity at  $T_c$  near 1483 K, the structure remains  
16 trigonal, but the inversion symmetry of the system is lifted, reducing the symmetry to  
17 the  $R3c$  space group. LiNbO<sub>3</sub> is hence ferroelectric but not ferroelastic below 1483 K.  
18  
19 Domain structures consist exclusively of 180° ferroelectric walls, which are almost  
20 strain-free in thermodynamic equilibrium while weak local strains originate from  
21 coupling between the polarization and secondary displacements of the oxygen  
22 cages.<sup>[30,31]</sup> The crystallographic properties and energetics of domain walls in LiNbO<sub>3</sub>  
23  
24 have been described in great detail in [31,32], we refer the reader to the excellent  
25 review in [31] for further details. In the present paper we confirm the presence of  
26 domain wall meanders even in LiNbO<sub>3</sub> without engineered inclined walls and  
27 demonstrate, for the first time, that head-to-head configurations exist in a nominally  
28 ‘straight’ domain wall. This observation confirms that local charges occur inside  
29 domain walls in LiNbO<sub>3</sub>.  
30  
31  
32  
33  
34  
35  
36  
37  
38  
39  
40  
41  
42  
43  
44  
45  
46  
47  
48  
49  
50  
51  
52  
53  
54  
55  
56  
57  
58  
59  
60  
61  
62  
63  
64  
65

## 2. Results and discussion

LiNbO<sub>3</sub> is an electron beam-sensitive material. Therefore, both the TEM specimen preparation and the HAADF-STEM image acquisition were optimized in order to obtain most reliable TEM data. The most optimal FIB lamella (**Figure 1b**) had a thickness of about 70 nm (estimated using electron energy loss spectroscopy), which is a compromise between the electron transparency and the ion-beam damage during the sample preparation. The HAADF-STEM data were collected along the  $[1\bar{1}00]$  direction, as a time series of 49 frames with a very short acquisition time of 2.5 s per frame. This mode significantly reduces the dose rate, improving the stability of the material under the electron beam, and minimizes the effect of mechanical instabilities of the sample during the experiment.

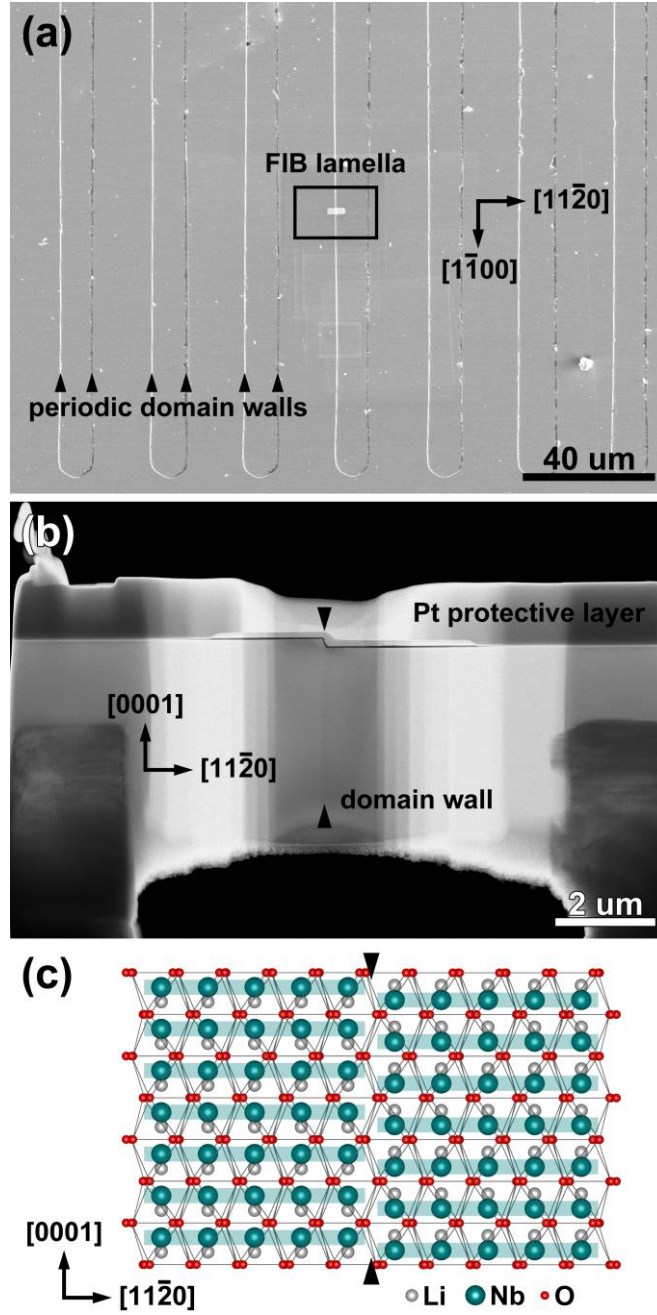


**Figure 1.** a) Overview SEM image of the investigated LiNbO<sub>3</sub> crystal viewed normal to the surface, i.e., along the [0001] direction. Induced domain walls appear as a set of periodic parallel lines. The site where the FIB specimen was extracted can be seen as a bright narrow strip of the Pt protective layer. b) Low magnification HAADF-STEM image of an optimized FIB lamella, viewed along the [1 $\bar{1}$ 00] direction. The domain wall (marked with arrowheads) can be recognized as a thin straight line of weaker intensity running along the [0001] direction and located right under the surface step.



1  
2  
3  
4  
5  
6  
7  
8  
9  
c) Idealised schematic illustration of the domain wall, assuming the oxygen sublattice  
10  
11  
12  
13  
14  
15  
16  
17  
18  
19  
20  
21  
22  
23  
24  
25  
26  
27  
28  
29  
30  
31  
32  
33  
34  
35  
36  
37  
38  
39  
40  
41  
42  
43  
44  
45  
46  
47  
48  
49  
50  
51  
52  
53  
54  
55  
56  
57  
58  
59  
60  
61  
62  
63  
64  
65  
to remain unchanged when crossing the domain wall. Rows of Nb atomic columns are  
highlighted with teal stripes.

The acquired data were processed using the Smart Align software package.<sup>[33]</sup>  
First, all the frames were aligned with respect to each other to compensate for the  
mechanical drift during the acquisition. Then, each frame was individually corrected  
for the scan distortions. In the end, the frames were combined into a single image with  
improved signal-to-noise ratio and minimized scan and drift distortions. A  
representative fragment of the averaged image is shown in **Figure 2a**. The position of  
the ferroelectric domain wall is marked with a white arrow, and can be seen as a strip  
with a slightly lower intensity. Also, it creates a weak ripple in the rows of white dots  
when looking at this image along a grazing incidence from left to right. In the  
HAADF-STEM images the signal is dependent on the chemical composition of the  
projected atomic columns and scales as  $I \sim Z^{1.6-1.9}$ , where  $Z$  is an average atomic  
number. Therefore, in the  $[1\bar{1}00]$  HAADF-STEM images of  $\text{LiNbO}_3$ , the projected  
Nb-Li ( $Z[\text{Nb}] = 41$ ,  $Z[\text{Li}] = 3$ ) columns appear as bright dots arranged into a  
rectangular pattern, while the O ( $Z[\text{O}] = 8$ ) columns are not visible. In the following  
the Nb-Li columns are referred to as Nb columns since simulations have shown that,  
as can be expected, the Li atoms are too light to cause any visible effect in the  
imaging.

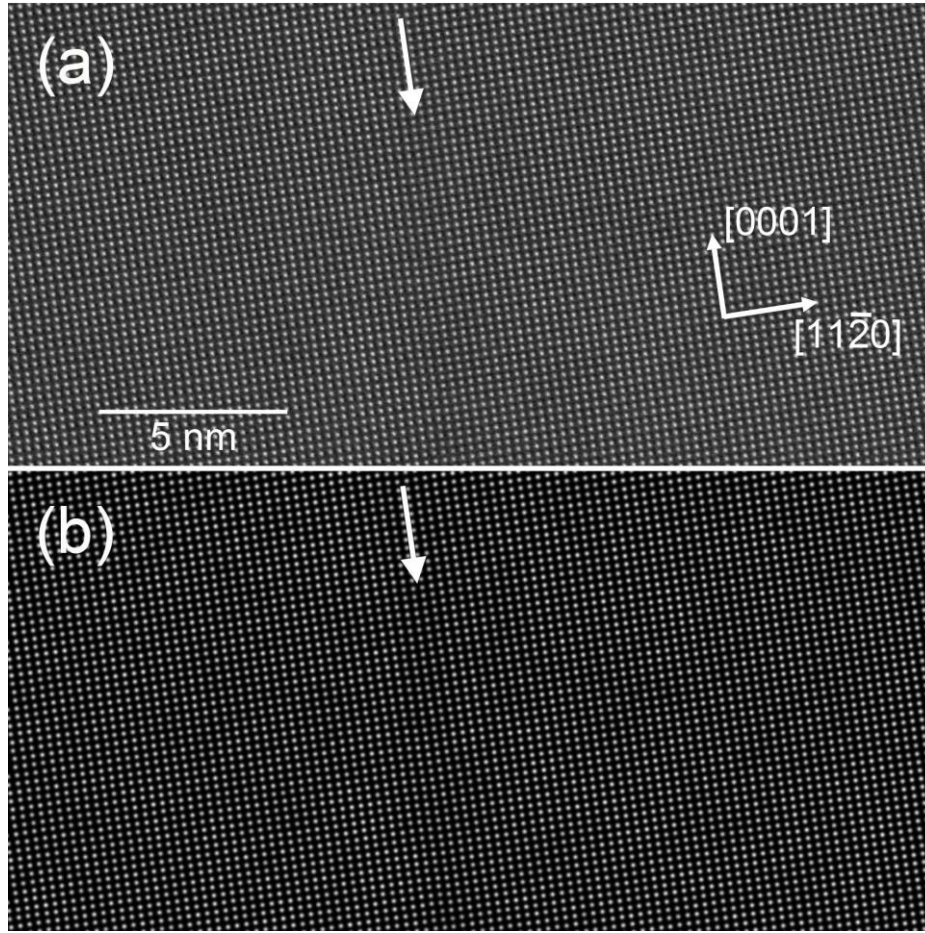


**Figure 2.** a) The  $[1\bar{1}00]$  HAADF-STEM image of the ferroelectric domain wall area in the  $\text{LiNbO}_3$  sample, averaged over 49 frames and corrected for the drift and scan distortions. b) The fitted model of the HAADF-STEM image. The arrows indicate the direction and location of the interface.

To analyse the Nb atomic displacements at the ferroelectric domain wall the projected 2D coordinates of the Nb columns in the averaged  $[1\bar{1}00]$  HAADF-STEM image were determined using statistical parameter estimation theory.<sup>[34-36]</sup> The image was fitted with a parametric model in which the intensity distribution of each atomic column in the image is described as a Gaussian function, peaked at the column position. The parameters of this model, including the positions, height, and width of the Gaussian peaks, were determined using the least-square estimator. The refined

model is shown in Figure 2b, where the position of the domain wall is again indicated with a white arrow.

For the determination of the Nb positions we assume that the ferroelectric domain wall does not change the anion sublattice of the structure, but inverts the ferroelectric displacements of the Nb cations. The inverted Li positions cannot be extracted from the images because the Li atomic scattering factor is much smaller than Nb so that all observed displacements are nominally related to Nb. The following procedure was employed to identify the pattern of cation displacements and the sideways displacements, if any, of the domain wall along the  $[11\bar{2}0]$  direction. First, a region of 90 atomic rows was selected along the  $[0001]$  direction, each of which measuring 59 atomic columns along the  $[11\bar{2}0]$  direction (this region is the shaded rectangle in **Figure 3a**). Then, for each row of 59 columns two reference lines were fitted by linear regression, using the coordinates of the 15 Nb columns at both ends of the row on either side of the wall (green lines in Figure 3b). In this fit, the slope of the reference lines for a given row at both sides of the domain wall was restricted to be the same, whereas the intercept with the interface was allowed to vary. The slopes for different atomic rows were not restricted.

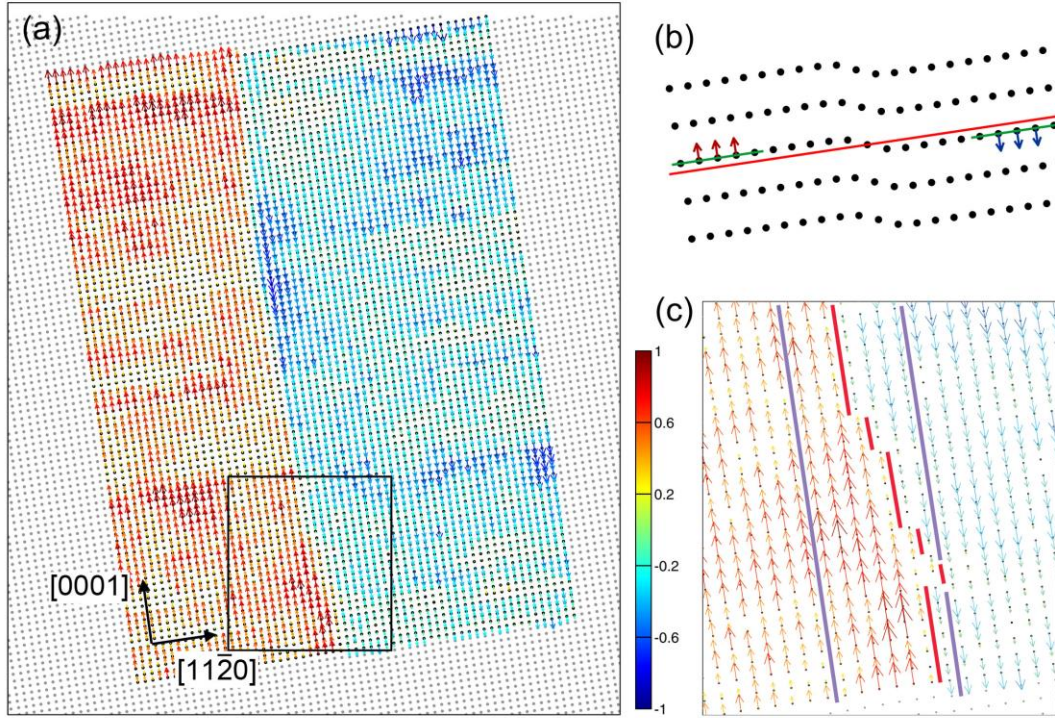


**Figure 3.** a) The analyzed region of 90 reference atomic rows: grey dots correspond to the fitted atom column positions, red and blue arrows indicate the displacement of the fitted atomic positions with respect to the base line and pointing in the direction of the displacement (the larger the displacement, the darker and longer the arrow). b) Schematic (stretched in the  $[0001]$  direction for clarity) showing green reference lines fitted to reference Nb columns in each ferroelectric domain and the red base line midway those reference lines. c) Enlargement of the squared area in a), where now the straight domain wall segments are indicated in red. Purple lines indicate the transition region, where the Nb displacements are inverted (i.e., the overall width of the domain wall). Another sample image from a different part of the interface is shown in **Figure S1** of the supplementary information.

To calculate the ferroelectric displacements of the Nb atoms, a base line for every  $[11\bar{2}0]$  atomic row was then defined midway both reference lines (red line in



Figure 3b, which has the same slope as both fitted green reference lines). The red line represents the approximate position of Nb in the paraelectric phase. Then, the Nb displacement from the red line for each column was calculated for each Nb column. This displacement represents the approximate ferroelectric shift of Nb. By design this implies that we only measure the displacements of the Nb columns along the [0001] direction, i.e., parallel to the  $(11\bar{2}0)$  domain wall. In Figure 3 the displacements are represented with the vectors pointing in the direction of the displacement.

The location of the domain wall along the  $[11\bar{2}0]$  direction in a given row of Nb atomic columns can be determined as the point where the polar displacements of Nb columns change direction. The location points of the domain wall do not form perfectly straight lines along [0001], but meander back and forth along the  $[11\bar{2}0]$  direction. Nevertheless, straight segments of the domain wall can be identified (red lines in Figure 3c). The overall meanders and local kinks between the wall segments occur within a narrow region of about 7 unit cells along the  $[11\bar{2}0]$  direction, represented by the purple full lines in Figure 3c. On a mesoscopic length scale, the domain wall is well confined to the  $(11\bar{2}0)$  plane.

Having quantified the off-center displacement of the Nb columns near the ferroelectric domain wall, the width of the wall in each of the 90 selected Nb rows was analysed using a simple parametric model:<sup>[37]</sup>

$$f(\beta_1, \beta_2, \beta_3, \beta_4) = \beta_1 + \beta_2 \tanh\left(\frac{x - \beta_3}{\beta_4}\right) \quad (1)$$

where  $x$  represents the coordinates of the fitted atomic columns along  $[11\bar{2}0]$  in a single Nb column row,  $\beta_1$  corresponds to the position of the domain wall midpoint along the [0001] direction, i.e., the base line of the atomic row (red line in Figure 3b),  $\beta_2$  corresponds to the distance between the base line and the corresponding reference lines,  $\beta_3$  denotes the position of the domain wall midpoint along  $[11\bar{2}0]$ , and  $\beta_4$

represents the half-width of the transition region of the domain wall along  $[11\bar{2}0]$ . In the model, the width of the domain wall corresponds to  $2\beta_4$  and it is independent of the actual location of the interface within the row ( $\beta_3$ ).

Analysis of the calculated widths of the domain walls for all 90 atomic rows demonstrates that there are two characteristic ranges of the wall widths (see the corresponding histogram S2 in the supplementary information). Most of the rows have a very narrow width of the domain wall, showing a step-like behaviour of Nb displacements. However, nine rows show much wider widths of up to about 20 unit cells, which could be due to a meandering of the interface along the viewing direction.

Considering only the atomic rows that demonstrate a sharp transition in the Nb off-centre displacements across the domain wall, an average wall width of  $174 \text{ pm} \pm 33 \text{ pm}$  was calculated. Alternatively, an averaged master curve for the Nb displacements in the entire region of interest was constructed. The atomic rows were first aligned with respect to each other along the  $[11\bar{2}0]$  direction, to compensate for the side-ways meanders in the position of the wall. The obtained master curve for the whole region is shown in **Figure 4**. The dots correspond to the averaged atomic column positions for a given row. The curve represents the fitted parametric model, which also estimates the averaged domain wall width as 174 pm. The master curve illustrates that on average the domain wall is associated with sharp transitions in the polar displacements of the Nb atoms, accounting for just 3 unit cells along the  $[11\bar{2}0]$  direction. Besides, the average displacements of the first atoms on either side of the wall from the base line are estimated as 9.4 pm, which is only slightly lower than the average value of 12.48 pm for the rest of the row and confirms the sharpness of the averaged interface. In a recent work, Wei et al. found a width of 7 pseudocubic unit cells and an averaged lead atom displacement of 8 pm at anti-phase boundaries in

PbZrO<sub>3</sub> using negative spherical aberration imaging and averaging over selected atomic rows, but without using parameter estimation theory.<sup>[38]</sup>

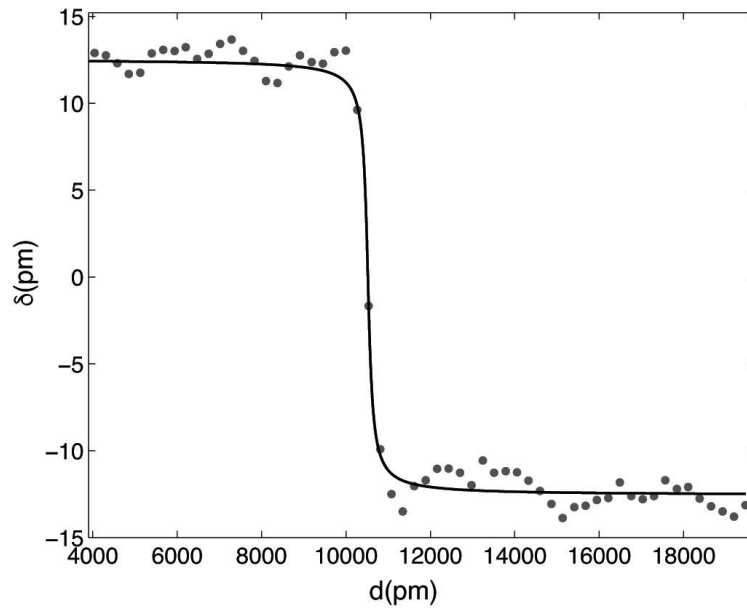


**Figure 4.** The master curve of Nb displacements in the analyzed region (dots) and the corresponding fitted parametric model (curve).

The main structural features of the wall in Figure 3c are the kinks of the displacements by one unit cell. While the overall direction is well defined, one could define the mesoscopic wall width as the distance between the two purple limiting lines (7 unit cells). Over rather long distances, the wall position does not fluctuate beyond this corridor. This situation is very different on a truly atomic scale where kinks with a step of one unit cell are rather common. Only these kinks produce local charges whenever two dipoles with opposite directions meet at a kink of the wall. These kinks can have a high density with 5 kinks over 26 unit cells along the [0001] direction while they are less common in other parts of the sample. If all kinks in the section seen in Figure 3c were oriented in the same direction, the wall would be inclined by a fraction of degree. Such walls were shown to exhibit Cherenkov second

1 harmonic generation (CSHG) and various fine structures of domain walls have been  
2 made visible optically.<sup>[17,39,40]</sup>  
3

4 While the macroscopic wall inclination is strictly zero, the local inclinations  
5 and hence the number of kinks is large in our sample. This implies that the local wall  
6 conductivity (hopping) is large, but we do not expect large distance electronic  
7 transport because straight wall segments act as insulators between the kink-rich  
8 regions. This picture of local electronic resonances was advocated previously and our  
9 results fully support these findings.<sup>[27,41]</sup> Our results are also in agreement with the  
10 lack of conductivity of domain walls with a macroscopic inclination of zero.<sup>[16]</sup>  
11 Furthermore, the presence of a large number of kinks means that the domain wall is a  
12 rough interface and will sensibly affect the CSHG signal.  
13  
14  
15  
16  
17  
18  
19  
20  
21  
22  
23  
24  
25

26 From the pairs of reference lines for each  $[11\bar{2}0]$  row of atomic columns in  
27 Figure 3, the average shift between the Nb atoms across the domain wall equals 25.0  
28 pm with a standard error of 1.1 pm (i.e., the distance between the stripes of  $[11\bar{2}0]$  Nb  
29 rows along the  $[0001]$  direction in Figure 1c). This value is about half of the expected  
30 value of ca. 55 pm calculated from the crystallographic bulk data of  $\text{LiNbO}_3$  (see  
31 **Table S1** in the supporting information). However, the spontaneous polarization and  
32 hence the Nb shift of 24 pm in the TEM sample is that of a thin film prepared by FIB,  
33 so it can be expected to be reduced with respect to the bulk value. This effect may be  
34 a genuine size effect or related to strain and topological disorder along the beam  
35 direction, which could also result in the heterogeneities in the displacements as seen  
36 away from the domain wall in Figure 3a. Nevertheless, all topological features of the  
37 domain wall appear to be the same as in bulk samples. To further test whether the  
38 patches of small and large displacements visible in Figure 3 are due to heterogeneous  
39 strain effects, the Nb shifts with respect to the position extrapolated from the four  
40  
41  
42  
43  
44  
45  
46  
47  
48  
49  
50  
51  
52  
53  
54  
55  
56  
57  
58  
59  
60  
61  
62  
63  
64  
65



nearest neighbor sites were calculated.<sup>[42]</sup> This does indeed average the strain variable as seen in **Figure S4** and thus largely eliminates the heterogeneities.

The agreement with findings of optical and conductivity investigations lead to a follow up question: to which extend are the local kinks stable or do they represent unstable states which change in time? To investigate such possible dynamics of the observed ferroelectric domain, the image processing and data analysis procedure described above were also performed on smaller sets of data, i.e., on the HAADF-STEM images averaged over the first 24 and last 24 frames. Taking precision ranges into account, in about 90% of the rows the measured position of the interface did not move between the first 24 and last 24 frames (**Figure S3**). Some of the rows that showed a changing location of the interface are located in areas where the interface width (i.e.,  $2\beta_4$ ) was found to be about 20 unit cells (cfr. **Figure S2**), but others were located at rows with a sharp interface. At present, it is thus unclear whether or not this observation is due to any dynamics of the system within the timeframe of 125 s of the experiment, but it appears possible that such instabilities exist.<sup>[43]</sup> It may be a possible next step towards the identification of such time dependences to make use of the CSHG radiation as function of time.

### 3. Conclusions

We have shown that ferroelectric domain walls in  $\text{LiNbO}_3$  follow, within experimental resolution, the predictions for  $180^\circ$  walls. Even for equilibrated walls, we find that the wall locally meanders yielding local wall directions inclined with respect to the ferroelectric polarization. These meanders generate kinks and dipolar configurations where the ferroelectric dipoles are oriented head-to-head or tail-to-tail.

1 These configurations necessarily induce local charges, which do not destabilize the  
2 overall wall configuration.  
3  
4  
5  
6  
7  
8  
9

#### 10 **4. Experimental Section**

11 The original material is a congruent periodically poled single crystal, commercially  
12 available from EQ Photonics GmbH (labelled as PPLNb in [29]). It has been poled at  
13 room temperature, with an experimental arrangement similar to the one described by  
14 Myers et al.<sup>[44]</sup> To identify the position of the domain wall, the sample was  
15 subsequently etched with HF, resulting in a height difference between adjacent  
16 domains (Figure 1a and 1b).<sup>[45]</sup> These preparative steps were performed by the  
17 supplier.  
18

19 The pattern of atomic displacements at the ferroelectric domain wall in LiNbO<sub>3</sub> was  
20 observed using high angle annular dark field scanning transmission electron  
21 microscopy (HAADF-STEM). The TEM specimens were prepared using focused ion  
22 beam (FIB) with a dual-beam FEI Helios Nanolab 650 instrument. FIB lamellae were  
23 cut along the [0001] crystallographic direction (i.e., normal to the crystal surface) and  
24 perpendicular to the domain wall (Figure 1a). In this orientation, when analyzed with  
25 TEM, the samples provide a clear view of the atomic structure along the  $[1\bar{1}00]$   
26 crystallographic direction, i.e., parallel to the  $(11\bar{2}0)$  domain wall. HAADF-STEM  
27 images were acquired with an FEI Titan<sup>3</sup> 60-300 probe aberration corrected  
28 microscope operated at 300 kV, with a probe semi-convergence angle of 21 mrad, a  
29 probe current of 40 pA and the inner angle of the annular detector set at 58 mrad.  
30  
31  
32  
33  
34  
35  
36  
37  
38  
39  
40  
41  
42  
43  
44  
45  
46  
47  
48  
49  
50  
51  
52  
53  
54  
55  
56  
57  
58  
59  
60  
61  
62  
63  
64  
65

## Acknowledgements

JG acknowledges the support from the Research Foundation Flanders (FWO, Belgium) through various project fundings (G.0368.15N, G.0369.15N and G.0374.13N), as well as financial support from the European Union Seventh Framework Programme (FP7/2007-2013) under Grant agreement no. 312483 (ESTEEM2). The authors thank J. Hadermann for useful suggestions on the interpretation of the HAADF-STEM images. EKHS thanks EPSRC (EP/K009702/1) and the Leverhulme trust (EM-2016-004) for support. GFN thanks the National Research Fund, Luxembourg (FNR/P12/4853155/Kreisel) for support.

## References

- [1] E. K. H. Salje, *ChemPhysChem* **2010**, *11*, 940.
- [2] J. Seidel, P. Maksymovych, Y. Batra, A. Katan, S.-Y. Yang, Q. He, A. P. Baddorf, S. V. Kalinin, C.-H. Yang, J.-C. Yang, Y.-H. Chu, E. K. H. Salje, H. Wormeester, M. Salmeron, R. Ramesh, *Phys. Rev. Lett.* **2010**, *105*, 197603.
- [3] S. Farokhipoor, B. Noheda, *Phys. Rev. Lett.* **2011**, *107*, 127601.
- [4] O. Diéguez, P. Aguado-Puente, J. Junquera, J. Íñiguez, *Phys. Rev. B* **2013**, *87*, 024102.
- [5] J. Guyonnet, I. Gaponenko, S. Gariglio, P. Paruch, *Adv. Mater.* **2011**, *23*, 5377.
- [6] A. Aird, E. K. H. Salje *J. Phys.: Condens. Matter* **1998**, *10*, L377.
- [7] Y. Kim, M. Alexe, E. K. H. Salje, *Appl. Phys. Lett.* **2010**, *96*, 032904.
- [8] H. Yokota, H. Usami, R. Haumont, P. Hicher, J. Kaneshiro, E. K. H. Salje, Y. Uesu, *Phys. Rev. B* **2014**, *89*, 144109.
- [9] S. Van Aert, S. Turner, R. Delville, D. Schryvers, G. Van Tendeloo, E. K. H. Salje, *Adv. Mater.* **2012**, *24*, 523.
- [10] E. K. H. Salje, O. Aktas, M. A. Carpenter, V. V. Laguta, J. F. Scott, *Phys. Rev. Lett.* **2013**, *111*, 247603.
- [11] J.F. Scott, E.K.H. Salje, M.A. Carpenter *Phys. Rev. Lett.* **2012**, *109*, 187601.

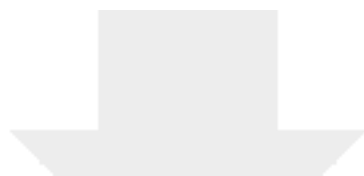
- [12] S. Farokhipoor, C. Magén, S. Venkatesan, J. Íñiguez, C. J. M. Daumont, D. Rubi, E. Snoeck, M. Mostovoy, C. de Graaf, A. Müller, M. Döblinger, C. Scheu, B. Noheda, *Nature* **2014**, 515, 379.
- [13] A. Y. Borisevich, O. S. Ovchinnikov, H. Jung Chang, M. P. Oxley, P. Yu, J. Seidel, E. A. Eliseev, A. N. Morozovska, R. Ramesh, S. J. Pennycook, S. V. Kalinin, *ACS Nano* **2010**, 4, 6071.
- [14] J. Seidel, L. W. Martin, Q. He, Q. Zhan, Y.-H. Chu, A. Rother, M. E. Hawkrige, P. Maksymovych, P. Yu, M. Gajek, N. Balke, S. V. Kalinin, S. Gemming, F. Wang, G. Catalan, J. F. Scott, N. A. Spaldin, J. Orenstein, R. Ramesh, *Nat. Mater.* **2009**, 8, 229.
- [15] M. Schröder, A. Haußmann, A. Thiessen, E. Soergel, T. Woike, L. M. Eng, *Adv. Funct. Mater.* **2012**, 22, 3936.
- [16] M. Schröder, X. Chen, A. Haußmann, A. Thiessen, J. Poppe, D. A. Bonnell, L. M. Eng, *Mater. Res. Express* **2014**, 1, 035012.
- [17] T. Kämpfe, P. Reichenbach, M. Schröder, A. Haußmann, L. M. Eng, T. Woike, E. Soergel, *Phys. Rev. B* **2014**, 89, 035314.
- [18] E. A. Eliseev, A. N. Morozovska, G. S. Svechnikov, V. Gopalan, V. Y. Shur, *Phys. Rev. B* **2011**, 83, 235313.
- [19] C.-L. Jia, S.-B. Mi, K. Urban, I. Vrejoiu, M. Alexe, D. Hesse, *Nat. Mater.* **2008**, 7, 57.

- [20] V. Aristov and L. Kokhanchik, *Ferroelectrics*, **1992**, 126, 353.
- [21] V. V. Aristov, L. S. Kokhanchik, and Y. I. Voronovskii, *Phys. Status Solidi*, **1984**, 86, 133.
- [22] L. S. Kokhanchik, *Micron*, **2009**, 40, 41.
- [23] G. Catalan, J. Seidel, R. Ramesh, J. F. Scott, *Rev. Mod. Phys.* **2012**, 84, 119.
- [24] G. F. Nataf, O. Aktas, T. Granzow, Torsten, E. K. H. Salje, *J. Phys.: Condens. Matter* **2016**, 28, 015901.
- [25] H. Xu, D. Lee, J. He, S. Sinnott, V. Gopalan, V. Dierolf, S. Phillpot, *Phys. Rev. B* **2008**, 78, 174103.
- [26] S. C. Abrahams and P. Marsh, *Acta Crystallogr. Sect. B Struct. Sci.*, **1986**, 42, 61.
- [27] P. Lerner, C. Legras, J. P. Dumas, *J. Cryst. Growth* **1968**, 3, 231.
- [28] H. Xu, D. Lee, S. B. Sinnott, V. Gopalan, V. Dierolf, S. R. Phillpot, *IOP Conf. Ser. Mater. Sci. Eng.* **2010**, 15, 012003.
- [29] G. Stone, D. Lee, H. Xu, S. R. Phillpot, V. Dierolf, *Appl. Phys. Lett.* **2013**, 102, 042905.
- [30] Morozovska, and N. Setter, *Phys. Rev. Lett.*, **2014**, 113, 207601.
- [31] V. Gopalan, V. Dierolf, and D. A. Scrymgeour, *Annu. Rev. Mater. Res.* **2007**, 37, 449.

- [32] L. Donghwa, X. Haixuan, D. Volkmar, V. Gopalan, S. R. Phillpot, *Phys. Rev. B* **2010**, 82, 014104.
- [33] L. Jones, H. Yang, T. Pennycook, M. Marshall, S. Van Aert, N. Browning, M. Castell, P. D. Nellist, *Adv. Struct. and Chem. Imag.* **2015**, 1, 8.
- [34] A.J. den Dekker, J. Gonnissen, A. De Backer, J. Sijbers, S. Van Aert, *Ultramicroscopy* **2013**, 134, 34.
- [35] A. J. den Dekker, S. Van Aert, A. van den Bos, D. Van Dyck, *Ultramicroscopy* **2005**, 104, 83.
- [36] S. Van Aert, J. Verbeeck , R. Erni, S. Bals, M. Luysberg, D. Van Dyck, G. Van Tendeloo, *Ultramicroscopy* **2009**, 109, 1236.
- [37] E. K. H. Salje, *Ann. Rev. of Mat. Res.* **2012**, 42, 265.
- [38] X.-K. Wei, A. K. Tagantsev, A. Kvasov, K. Roleder, C.-L. Jia, N. Setter, *Nat. Commun.* **2014**, 5, 3031.
- [39] Y. Sheng, A. Best, H. J. Butt, W. Krolikowski, A. Arie, K. Koynov, *Opt. Express* **2010**, 18, 16539.
- [40] T. Kämpfe, P. Reichenbach, A. Haußmann, T. Woike, E. Soergel, L. M. Eng, *Appl. Phys. Lett.* **2015**, 107, 152905.
- [41] A. Tselev, P. Yu, Y. Cao, L. R. Dedon, L. W. Martin, S. V. Kalinin, P. Maksymovych, *Nat. Commun.* **2016**, 7.

- [42] T. Jach, S. Kim, V. Gopalan, S. Durbin, D. Bright, *Phys. Rev. B* **2004**, *69*, 64113.
- [43] E. K. W. Salje, X. Wang, X. Ding, J. Sun, *Phys. Rev. B* **2014**, *90*, 064103.
- [44] L. E. Myers, R. C. Eckardt, M. M. Fejer, R. L. Byer, W. R. Bosenberg, J. W. Pierceet, *J. Opt. Soc. Am. B* **1995**, *12*, 2102.
- [45] C. L. Sones, S. Mailis, W. S. Brocklesby, R. W. Eason, J. R. Owen, *J. Mater. Chem.* **2002**, *12*, 295.





[Click here to access/download](#)

**Supporting Information**

**SupplInfo\_LiNbO3\_Submission.docx**

